

# Some nanograined ferrites and perovskites for catalytic combustion of acetone at low temperature

Nicolae Rezlescu<sup>a,\*</sup>, Elena Rezlescu<sup>a</sup>, Paul Dorin Popa<sup>a</sup>, Corneliu Doroftei<sup>a</sup>, Maria Ignat<sup>b</sup>

<sup>a</sup>National Institute of Research and Development for Technical Physics, Iasi, Romania

<sup>b</sup>“Al. I. Cuza” University, Faculty of Chemistry, Iasi, Romania

Received 16 September 2014; received in revised form 18 November 2014; accepted 25 November 2014

Available online 3 December 2014

## Abstract

Two types of nanograined oxide compounds,  $\text{CuFe}_2\text{O}_4$ ,  $\text{MgFe}_2\text{O}_4$ ,  $\text{Ni}_{0.5}\text{Co}_{0.5}\text{Fe}_2\text{O}_4$ , with spinel-type structure, and  $\text{SrMnO}_3$ ,  $\text{FeMnO}_3$ ,  $\text{La}_{0.6}\text{Pb}_{0.2}\text{Ca}_{0.2}\text{MnO}_3$  with perovskite-type structure, were prepared by sol–gel self-combustion method and tested for the catalytic combustion of dilute acetone in air. Their structure and surface properties were investigated by X-ray diffraction (XRD), scanning electron microscopy (SEM), BET surface area measurements and energy-dispersive X-ray spectroscopy (EDX). We chose acetone as a VOC model because, among all VOCs, it is a common organic solvent extensively used in the manufacture of plastics, fibers, drugs and other chemicals. The catalytic activity studies revealed that between these two types of catalysts, the perovskite catalysts exhibited the best activity in the catalytic combustion of acetone. The acetone conversion degree over perovskite catalysts can exceed 95% at 300 °C, while over ferrosin catalysts it is of about 70%. Our experimental results indicate that the  $\text{SrMnO}_3$  and  $\text{La}_{0.6}\text{Pb}_{0.2}\text{Ca}_{0.2}\text{MnO}_3$  perovskites are the preferred catalysts in the catalytic combustion of acetone at low temperatures. The time stability of  $\text{La}_{0.6}\text{Pb}_{0.2}\text{Ca}_{0.2}\text{MnO}_3$  catalyst for acetone combustion was also investigated and no deactivation was observed for 36 h at 250 °C.

© 2014 Elsevier Ltd and Techna Group S.r.l. All rights reserved.

**Keywords:** Catalyst; Spinel structure; Perovskite structure. sol–gel; Self-combustion; Acetone combustion

## 1. Introduction

The removal of volatile organic compounds (VOCs) from air is important for environmental and human health [1,2]. Several technologies have been used to remove VOCs emissions [3,4]. The conventional thermal incineration requires high operating temperature ( $> 750$  °C) and significant energy amount. Catalytic combustion is the most promising method for release of VOCs [5–9] which operates at low temperature ( $< 500$  °C) and its efficiency is determined by the activity and stability of the catalyst used. Various kinds of catalysts, such as supported noble metals [10–12], metal oxides [13–15] or mixed metal oxides [16–20] can be employed. Transition metal oxides, although generally less active than noble metal, are

cheaper and more resistant to deactivation by poisoning than other materials [11,13,21,22].

In the last years much attention has been paid to the perovskite-type ceramic oxides,  $\text{ABO}_3$  (A is usually rare earth and B is transition metal [23–27]), and to the spinel ferrite-type oxides,  $\text{MFe}_2\text{O}_4$  (M is divalent metal ion) [28–31] as promising combustion catalysts mainly due to their excellent thermal stability properties, low cost and easy processing. Moreover, the structural stability of the perovskites allows for the partial substitution of A and/or B by other metal that can improve their catalyst properties.

The catalytic properties of the spinel ferrites are influenced by the cation distribution among the tetrahedral and octahedral sites in the spinel structure [31]. Jacobs et al. [32] suggested that in the spinel structure, the octahedral sites are almost exclusively exposed at the surface of the spinel crystallite and that the catalytic activity is mainly due to octahedral cations.

\*Corresponding author.

E-mail address: [nicolae.rezlescu@gmail.com](mailto:nicolae.rezlescu@gmail.com) (N. Rezlescu).

For catalytic purposes, the production of catalyst materials with nanosized particles is a priority. Nanograined ceramic materials present new opportunities for enhancing the performance of solid catalysts because of the much higher surface to bulk ratio compared to the coarse micrograined materials. Various methods have been proposed [33–37] to obtain catalyst materials with superior microstructure. In the present work we applied a nonconventional procedure, sol–gel coupled with self-combustion described in our previous papers [38,39]. This procedure offers a number of advantages including homogenous mixing on the atomic scale, high purity, simple equipment and control of the grain size by subsequent heat treatments.

Below we present a comparative study on the catalytic performances of the two nanocrystalline material types prepared by sol–gel self-combustion:  $\text{CuFe}_2\text{O}_4$ ,  $\text{MgFe}_2\text{O}_4$ ,  $\text{NiCoFe}_2\text{O}_4$  ferrites with spinel-type structure and  $\text{SrMnO}_3$ ,  $\text{FeMnO}_3$ ,  $\text{LaPbCaMnO}_3$  manganites with perovskite-type structure. The samples were characterized using X-ray diffraction (XRD), scanning electron microscopy (SEM), BET surface area measurements, and energy-dispersive X-ray spectroscopy (EDX). We analyzed the catalytic properties of the six samples, which have different compositions and structures, in the catalytic flameless combustion of dilute acetone. We have chosen acetone as a VOC model because, among all the VOCs, it is a common organic solvent extensively used in the manufacture of plastics, fibers, drugs and other chemicals.

## 2. Experimental

### 2.1. Sample preparation

Three nano-grained perovskite powders of nominal compositions:  $\text{SrMnO}_3$ ,  $\text{FeMnO}_3$ ,  $\text{La}_{0.6}\text{Pb}_{0.2}\text{Ca}_{0.2}\text{MnO}_3$  and three nano-grained ferros spinel powders of nominal compositions:  $\text{CuFe}_2\text{O}_4$ ,  $\text{MgFe}_2\text{O}_4$ ,  $\text{Ni}_{0.5}\text{Co}_{0.5}\text{Fe}_2\text{O}_4$  were prepared by sol–gel self-combustion procedure followed by heat treatment in the 900–1000 °C range (depending on the crystalline phase of materials). We used metal nitrates, ammonium hydroxide and polyvinyl alcohol (PVA) as starting materials. A solution containing metal nitrates was mixed with an aqueous solution (10% concentration) of polyvinyl alcohol. A small amount of  $\text{NH}_4\text{OH}$  solution (10% concentration) was dropped to adjust the pH value to about 8. This produced a sol of metal hydroxides and ammonium nitrate. By drying at 100 °C for 12 h, the sol was turned into a dried gel. The dried gel was ignited in a corner and a combustion reaction spontaneously propagated through the whole gel. The obtained powders were calcinated at 500 °C to eliminate the residual organic compounds. Finally, the calcined powders were annealed in air at 900 °C for 20 min (ferrite powders) and at 1000 °C for 320 min (perovskite powders). More details on the preparing procedure are given in [40].

### 2.2. Characterization techniques

The crystal structure and phase composition of the samples were analyzed by XRD. X-ray diffraction measurements of the powders were performed at room temperature using

PANALYTICAL X' PERT PRO MPD powder diffractometer and  $\text{CuK}\alpha$  radiation. The spectra were scanned between 20 and 80° (2 $\theta$ ) at a rate of 2°/min. The average crystallite size was evaluated based on XRD peak broadening using the Scherrer equation  $D = 0.9\lambda/\beta\cos\theta$ , where  $\lambda$  is radiation wavelength (0.15405 nm) of  $\text{CuK}\alpha$ ,  $\beta$  is the half width of the peak, and  $\theta$  is the Bragg diffraction peak angle. A scanning electron microscope (JEOL-200 CX) was used to visualize the surface morphology. NOVA 2200 apparatus was used to obtain  $\text{N}_2$  adsorption/desorption isotherms at 77 K. The BET specific surface area ( $S_{\text{BET}}$ ) was determined from nitrogen sorption data using the Brunauer–Emmett–Teller (BET) equation [41]. The elemental composition of the surface particles was examined with Energy Dispersive X-ray Spectrometer (Genesis, EDX) using a voltage of 20 kV.

### 2.3. Catalytic testing

Catalyst activity tests were conducted in a laboratory scale with a flow type set-up (flow rate of 100 cm<sup>3</sup>/min, acetone concentration in air of 1–2% and the gas hourly space velocity, GHSV, of 5100 h<sup>−1</sup>), previously described by us in [39,42]. The catalyst powder (0.3–0.5 g) was sandwiched between two layers of quartz wool in a quartz tubular micro-reactor ( $\phi=7$  mm) placed in an electrical furnace. The increase of the temperature was made in steps of 50 °C, from 50 °C to 550 °C. At every predetermined temperature, as a result of catalytic combustion, the gas concentration at the exit of reactor will be smaller than the inlet gas concentration. The catalytic activity of the heat treated materials under study was evaluated in terms of the conversion degree of the acetone over these materials as:

$$\text{Conv} = \frac{c_{\text{in}} - c_{\text{out}}}{c_{\text{in}}} \times 100\%,$$

where  $c_{\text{in}}$  and  $c_{\text{out}}$  are the inlet and outlet gas concentration, respectively, measured by a photo-ionization detector (PID-TECH) for VOCs. Data were collected when the flameless catalytic combustion had reached a steady state, after about 20 min at each temperature. These experiments were repeated decreasing the temperature and similar results were obtained, suggesting the stability of the ferrites and perovskites.

## 3. Results and discussion

### 3.1. Characterization of materials

XRD patterns of the six oxide compounds prepared by sol–gel self-combustion and heat treated are shown in Fig. 1. Diffractograms show well-defined peaks indicating a good crystalline quality of the powders. The broadening of the peaks indicates the generation of crystallites in the nano-size range. Phase identification was performed using PDF standard cards: for  $\text{MgFe}_2\text{O}_4$  (PDF # 17-464), for  $\text{CuFe}_2\text{O}_4$  (PDF # 34-425), for  $\text{NiCoFe}_2\text{O}_4$  (PDF # 44-1485 and # 22-1086), for  $\text{LaPbCaMnO}_3$  (PDF # 75-440), for  $\text{SrMnO}_3$  (PDF # 72-197) and for  $\text{FeMnO}_3$  (PDF # 75-1573). Results revealed that all samples

were monophase, without any second phase. The phase composition, lattice parameters and average crystallite size derived from XRD data are summarized in Table 1. One can see that the samples differ significantly in phase composition. Mg- and Ni/Co-ferrites belong to the cubic spinel structure, while Cu-ferrite crystallizes in a tetragonal distorted spinel (due to  $\text{Cu}^{2+}$  ions).  $\text{SrMnO}_3$  was indexed as hexagonal perovskite but the other two manganites have a cubic perovskite structure.

The lattice parameters match almost perfectly those presented in the literature in analogous compounds [43,44].

The size of the crystallites was found to be in the range 26–89 nm, proving the fine nature of the powders prepared by

sol–gel self-combustion. The smallest crystallites (25.8 nm) were identified in La–Pb–Ca containing manganite powder, while the Sr-manganite powder contained the largest crystallites (88.9 nm).

The surface morphology of the six powders can be observed in the SEM images given in Fig. 2. These micrographs reveal that, in all the studied systems, the nanometric particles ( $< 100$  nm) are clustered into mini- or macro-agglomerates with irregular shapes and sizes. Larger agglomerates are dispersed among small agglomerates. The images also reveal the presence of inter-agglomerate pores.

The elemental composition was checked by EDX analysis. It is known that EDX technique supplies an accurate determination of the atomic concentration of different elements present in the surface of the solid samples. In Fig. 3 we give EDX spectra for three catalyst materials only and their elemental compositions are summarized in Table 2. One can remark that the composition of the samples is similar to the nominal one, i.e. the  $\text{Cu}/(\text{Fe} + \text{Cu})$ ,  $\text{Fe}/(\text{Fe} + \text{Mn})$  and  $(\text{Ni} + \text{Co})/(\text{Fe} + \text{Ni} + \text{Co})$  ratios are close to the theoretical values given in parenthesis. This is proof of homogeneous distribution of the elements in the solids.

The nitrogen adsorption/desorption isotherms at 77 K of three samples are shown in Fig. 4. One can see that the desorption branch does not follow the adsorption branch, but forms a distinct hysteresis loop, which can be classified as an H3 type, according to the IUPAC classification [41]. Generally, this type of hysteresis loop is found in solids with agglomerates of particles. The BET specific surface areas ( $S_{\text{BET}}$ ), computed using the Brunauer–Emmett–Teller (BET) equation [41], are listed in Table 1. It should be noted that the perovskites and ferrites containing two cations, in contrast with samples containing more cations, have smaller values of  $S_{\text{BET}}$ ; this can be explained by an effective increase in degree of crystallinity during the heat treatment.

### 3.2. Catalyst activity

The catalyst activity of the prepared nanopowders was tested in the combustion reaction of acetone. The results are given in Fig. 5, where the measured values of acetone conversion are plotted as a function of the reaction temperature. Each datum is the average of three steady state measurements. Typical S-shaped curves were obtained, describing the variation of the conversion degree of acetone with increase of the reaction temperature. At decreasing

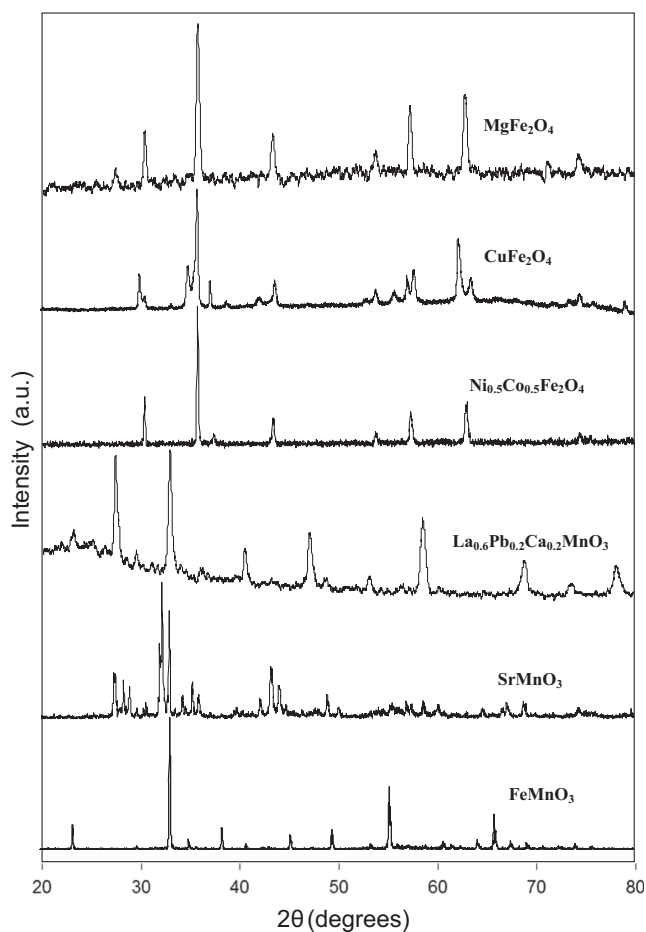


Fig. 1. Powder X-ray diffraction patterns of the investigated samples.

Table 1  
Structure characteristics of  $\text{MgFe}_2\text{O}_4$ ,  $\text{CuFe}_2\text{O}_4$ ,  $\text{Ni}_{0.5}\text{Co}_{0.5}\text{Fe}_2\text{O}_4$ ,  $\text{SrMnO}_3$ ,  $\text{FeMnO}_3$  and  $\text{La}_{0.6}\text{Pb}_{0.2}\text{Ca}_{0.2}\text{MnO}_3$ .

Catalyst composition	Phases by XRD analysis	Lattice parameter (nm)	$D_{\text{XRD}}$ (nm)	$S_{\text{BET}}$ ( $\text{m}^2/\text{g}$ )
$\text{MgFe}_2\text{O}_4$	Cubic spinel (space group $Fd3m$ )	$a=0.8366$	41.8	3.9
$\text{CuFe}_2\text{O}_4$	Tetragonal distorted spinel (space group $I41/amd$ )	$a=0.8000$ $c=0.8590$	36.0	1.5
$\text{Ni}_{0.5}\text{Co}_{0.5}\text{Fe}_2\text{O}_4$	Cubic spinel (space group $Fd3m$ )	$a=0.8365$	41.7	26.5
$\text{SrMnO}_3$	Hexagonal perovskite (space group $P63/mmc$ )	$a=0.5459$ $c=0.9090$	88.9	2.2
$\text{FeMnO}_3$	Cubic perovskite (space group $Ia3$ )	$a=0.9400$	59.2	3.2
$\text{La}_{0.6}\text{Pb}_{0.2}\text{Ca}_{0.2}\text{MnO}_3$	Cubic perovskite (Space group $Fm3m$ )	$a=0.7708$	26.8	12.6

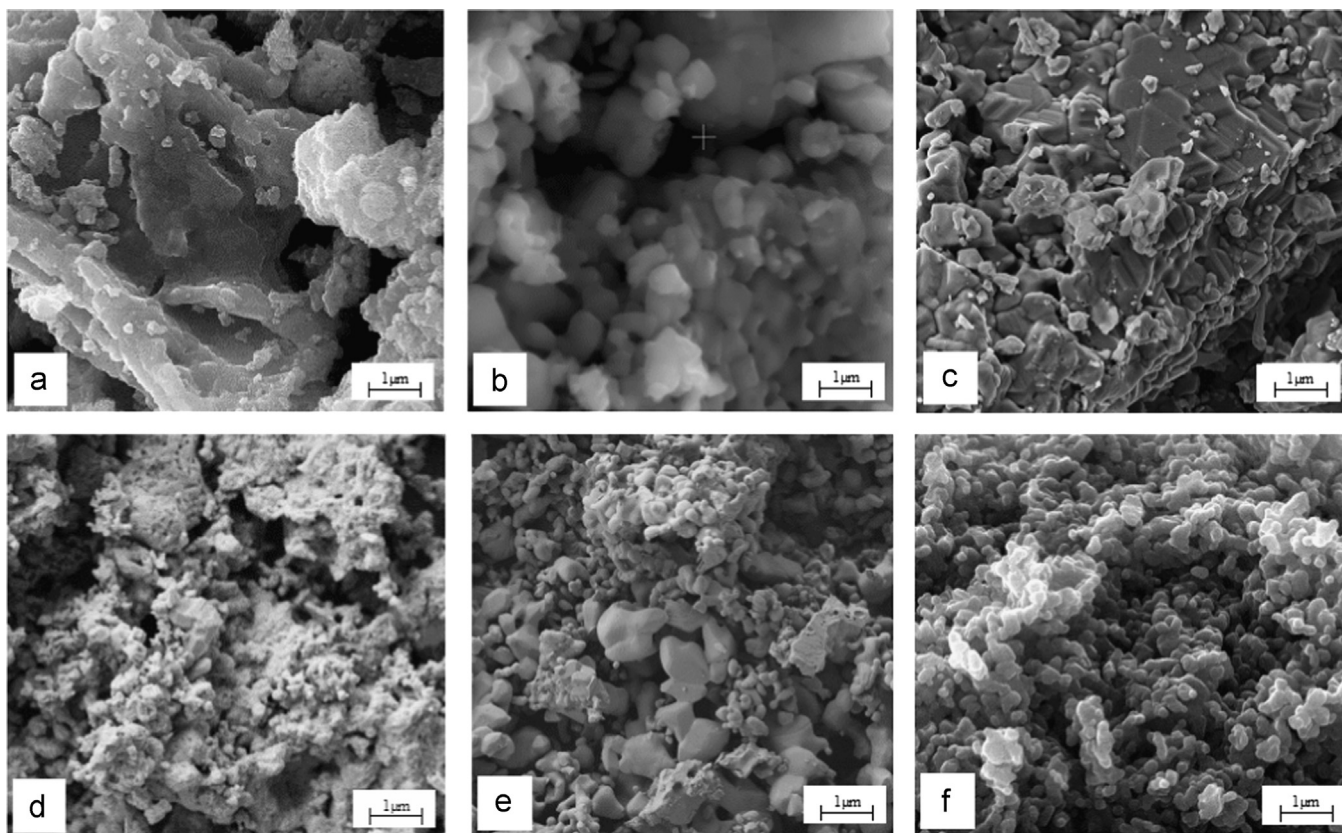


Fig. 2. SEM images of studied samples: (a)  $\text{MgFe}_2\text{O}_4$ ; (b)  $\text{CuFe}_2\text{O}_4$ ; (c)  $\text{Ni}_{0.5}\text{Co}_{0.5}\text{Fe}_2\text{O}_4$ ; (d)  $\text{SrMnO}_3$ ; (e)  $\text{FeMnO}_3$ ; (f)  $\text{La}_{0.6}\text{Pb}_{0.2}\text{Ca}_{0.2}\text{MnO}_3$ .

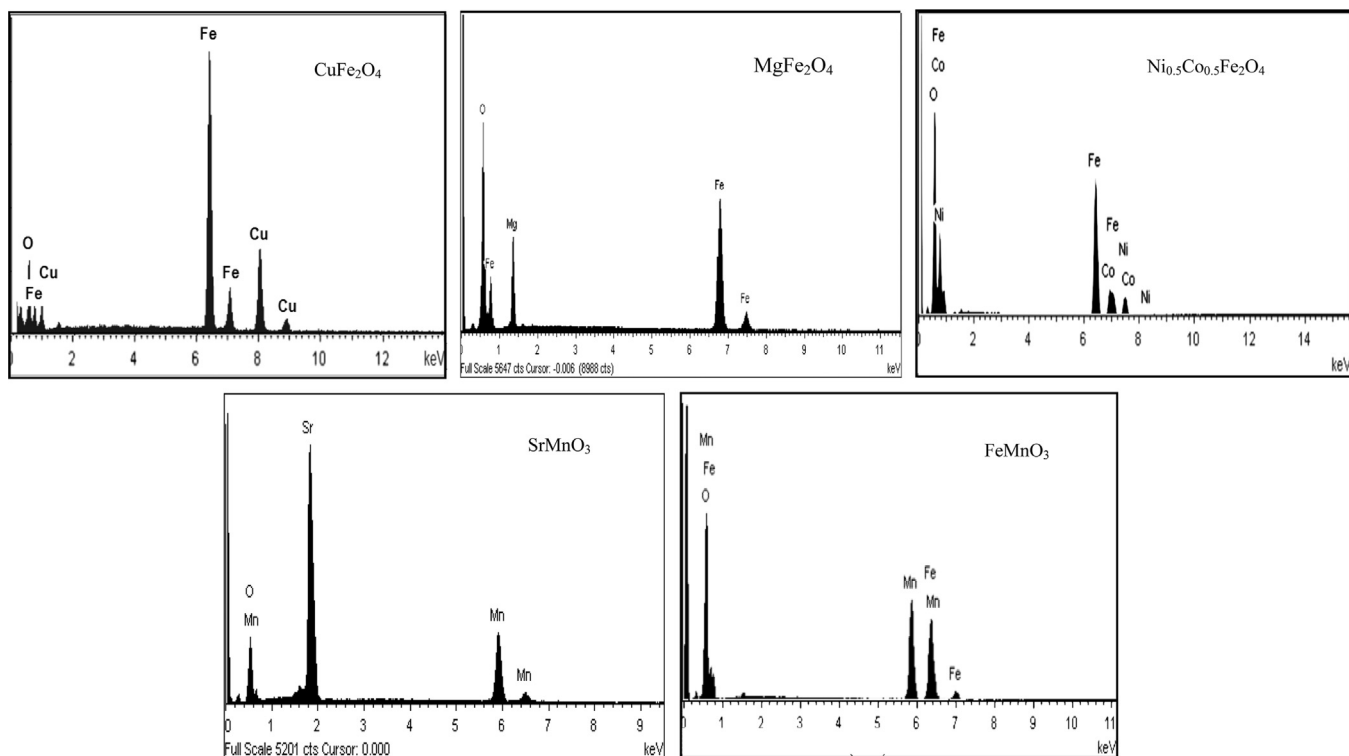


Fig. 3. EDX spectra for:  $\text{MgFe}_2\text{O}_4$ ,  $\text{CuFe}_2\text{O}_4$  and  $\text{Ni}_{0.5}\text{Co}_{0.5}\text{Fe}_2\text{O}_4$  ferrites heat treated at  $900^\circ\text{C}$  for 20 min,  $\text{SrMnO}_3$  and  $\text{FeMnO}_3$  perovskites heat treated at  $1000^\circ\text{C}$  for 320 min.

Table 2  
EDX analysis of the catalyst powders.

CuFe <sub>2</sub> O <sub>4</sub>		MgFe <sub>2</sub> O <sub>4</sub>		Ni <sub>0.5</sub> Co <sub>0.5</sub> Fe <sub>2</sub> O <sub>4</sub>		FeMnO <sub>3</sub>		SrMnO <sub>3</sub>		La <sub>0.6</sub> Pb <sub>0.2</sub> Ca <sub>0.2</sub> MnO <sub>3</sub>	
O (at%)	40.58	O (at%)	54.44	O (at%)	57.16	O (at%)	62.75	O (at%)	55.33	O (at%)	64.01
Cu (at%)	19.34	Mg (at%)	15.08	Ni (at%)	7.80	Fe (at%)	17.34	Sr (at%)	24.76	La (at%)	10.61
Fe (at%)	40.08	Fe (at%)	30.48	Co (at%)	8.06	Mn (at%)	19.91	Mn (at%)	20.03	Ca (at%)	3.42
				Fe (at%)	26.98					Pb (at%)	3.07
										Mn (at%)	18.90
Cu/(Fe + Cu)	0.32 (0.33)	Mg/(Mg + Fe)	0.33 (0.33)	(Ni + Co)/(Fe + Ni + Co)	0.37 (0.33)	Fe/(Mn + Fe)	0.47 (0.50)	Sr/(Mn + Sr)	0.55 (0.50)	Mn/(La + Ca + Pb + Mn)	0.52 (0.50)

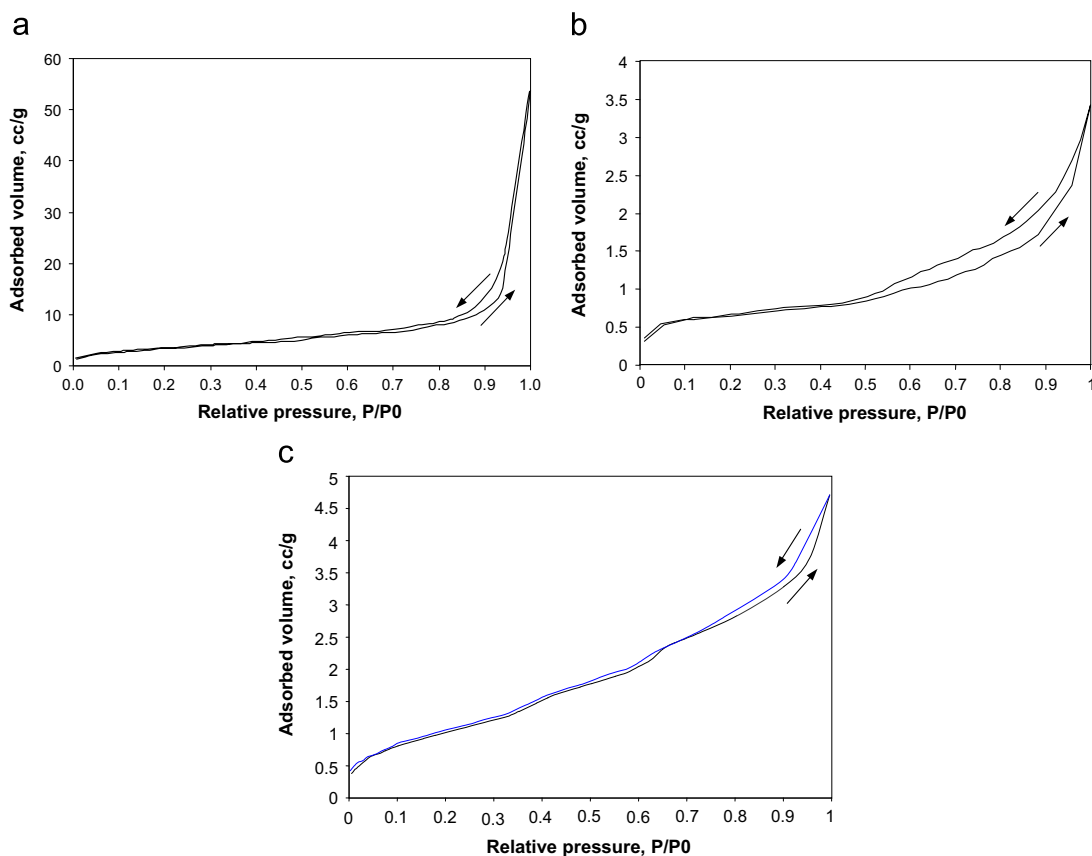


Fig. 4. Adsorption/desorption isotherm hysteresis loops of catalysts: (a) La<sub>0.6</sub>Pb<sub>0.2</sub>Ca<sub>0.2</sub>MnO<sub>3</sub>; (b) SrMnO<sub>3</sub>; (c) MgFe<sub>2</sub>O<sub>4</sub>.

temperature, the conversion levels of acetone are almost identical with those obtained at increasing temperature and *S*-shape curves superposed. These results show a good stability of the catalysts during the catalytic tests and the absence of any deactivation of the catalysts in all the experimental conditions tested.

The comparison of the obtained results revealed that the catalytic activities of the perovskite catalysts differ substantially from those of the ferrite catalysts. It is obvious in Fig. 5 that the *S*-curves involving perovskite catalysts are shifted to lower temperatures relative to those of ferrite catalysts. This means that the perovskite catalysts are more active in the acetone oxidation at low temperature than the ferrite catalysts. Also, it should be noted that the combustion reaction of acetone over perovskite catalysts starts at much lower temperatures (with about 100 °C) than over ferrite catalysts (except for Mg-ferrite)

and the conversion degree sharply increases with increasing temperature from 150 to 250 °C. The difference in the catalytic activity of the two catalyst systems cannot be explained by their different specific areas given in Table 1. Thus, the specific surface area of La<sub>0.6</sub>Pb<sub>0.2</sub>Ca<sub>0.2</sub>MnO<sub>3</sub> perovskite was 12.6 m<sup>2</sup>/g and that of Ni<sub>0.5</sub>Co<sub>0.5</sub>Fe<sub>2</sub>O<sub>4</sub> ferrite was 26.5 m<sup>2</sup>/g, but their activities differ strongly (Fig. 5).

An interesting result was obtained for two perovskite catalysts: SrMnO<sub>3</sub> and La<sub>0.6</sub>Pb<sub>0.2</sub>Ca<sub>0.2</sub>MnO<sub>3</sub> which have comparable catalytic activities over the whole temperature range, 50–550 °C. Regardless of the chemical composition, among all investigated catalysts the two perovskite catalysts exhibited the highest catalytic activity for acetone conversion. The perovskite catalysts were able to convert 95–97% acetone at low temperature, of 300 °C, whereas the conversion over ferrites was of about 65% only. The high

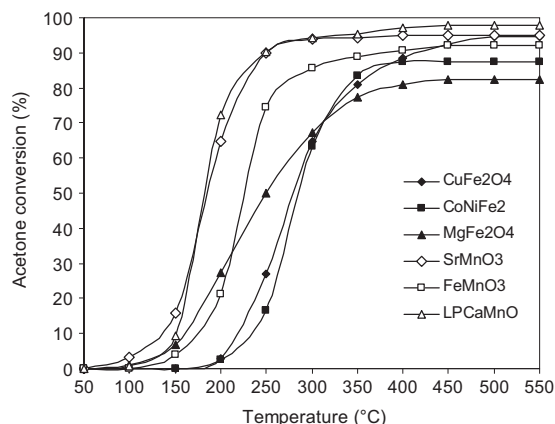


Fig. 5. Conversion versus temperature in the catalytic combustion of acetone over  $\text{MgFe}_2\text{O}_4$ ,  $\text{CuFe}_2\text{O}_4$ ,  $\text{Ni}_{0.5}\text{Co}_{0.5}\text{Fe}_2\text{O}_4$ ,  $\text{SrMnO}_3$ ,  $\text{FeMnO}_3$  and  $\text{La}_{0.6}\text{Pb}_{0.2}\text{Ca}_{0.2}\text{MnO}_3$  catalysts.

improved catalytic activity of the two manganites may be ascribed to the oxygen vacancies generated by the presence of both the manganese ions with variable valence [45,46] and the divalent ions ( $\text{Sr}^{2+}$ ,  $\text{Pb}^{2+}$ ,  $\text{Ca}^{2+}$ ).

In the case of the ferrite catalysts, higher temperature (400 °C) was required to achieve a large conversion (of about 89% for  $\text{CuFe}_2\text{O}_4$ ) as can be seen in Fig. 5. Moreover, one can remark that at about 300 °C the catalytic activities of the three ferrite catalysts are comparable, and for  $T > 300$  °C the activity of ferrites depends on the cation nature. From the obtained data one can conclude that the ferrites containing metal cations with variable valence are more active. Therefore, the higher catalytic activity of the Cu- and Ni/Co-ferrite catalysts than that of the Mg-ferrite at  $T > 300$  °C may be due to the multiple valences of Cu ( $\text{Cu}^{1+}$ – $\text{Cu}^{2+}$ ), Ni ( $\text{Ni}^{2+}$ – $\text{Ni}^{3+}$ ) and Co ( $\text{Co}^{2+}$ – $\text{Co}^{3+}$ ) ions [30], distributed on the octahedral sites in spinel structure. Florea et al. [29] showed by XPS analysis that the iron ion is mostly oxidized at  $\text{Fe}^{3+}$  state in Ni- and Mn-ferrites.

The effect of the crystalline structure and the chemical composition of the studied materials on the catalyst performances in acetone conversion at low temperature, of 250 °C, is apparent in Fig. 6. The best performances of the  $\text{SrMnO}_3$  and  $\text{La}_{0.6}\text{Pb}_{0.2}\text{Ca}_{0.2}\text{MnO}_3$  perovskite catalysts (90% conversion) may be related to the total or partial replacement of metal ion ( $\text{La}^{3+}$ ) by lower-valence ions ( $\text{Sr}^{2+}$  or  $\text{Pb}^{2+}$ – $\text{Ca}^{2+}$ ) in the  $\text{LaMnO}_3$  perovskite manganite. The condition of electro neutrality will imply the oxidation of  $\text{Mn}^{3+}$  to  $\text{Mn}^{4+}$  generating oxygen vacancies (active sites for oxygen adsorption) which enhance the catalytic activity of the perovskite manganites [45,46]. The lowest conversions (27% and 17%, respectively) at 250 °C were achieved over  $\text{CuFe}_2\text{O}_4$  and  $\text{Ni}/\text{CoFe}_2\text{O}_4$  spinel ferrite catalysts. Higher activities of manganites compared to those of ferrites allow one to speculate that their crystalline structure and structural defects (oxygen vacancies) may account also for obtained results in the acetone combustion over the two material types (perovskites and ferrites).

The catalytic activity of the catalysts in the VOC conversion can be estimated by three performance indices:  $T_{10}$  (the

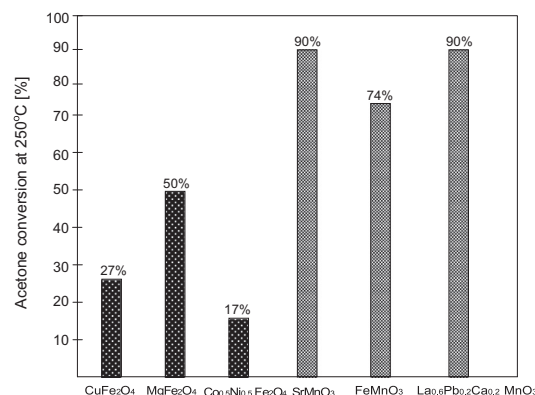


Fig. 6. Acetone conversion (%) at 250 °C over the two types of oxide compound catalysts: ferrosinels and perovskites.

Table 3

Temperatures (°C) of 10%, 50% and 90% acetone conversion, conversion degree at 400 °C, apparent activation energy and reaction rate over studied catalysts.

Catalyst composition	$T_{10}$ (°C)	$T_{50}$ (°C)	$T_{90}$ (°C)	Gas conversion (%)	Activation energy (kJ/mol)	Reaction rate ( $\mu\text{mol/s m}^2$ )
$\text{MgFe}_2\text{O}_4$	165	250	–	81	85.5	$8.14 \times 10^{-2}$
$\text{CuFe}_2\text{O}_4$	220	278	415	89	102.2	$15.9 \times 10^{-2}$
$\text{Ni}_{0.5}\text{Co}_{0.5}\text{Fe}_2\text{O}_4$	235	282	–	87	80.0	$1.35 \times 10^{-2}$
$\text{SrMnO}_3$	135	185	250	95	37.0	$140.0 \times 10^{-2}$
$\text{FeMnO}_3$	175	225	275	91	98.0	$65.0 \times 10^{-2}$
$\text{La}_{0.6}\text{Pb}_{0.2}\text{Ca}_{0.2}\text{MnO}_3$	150	180	250	97	68.5	$80.6 \times 10^{-2}$

temperature when VOC conversion is 10%),  $T_{50}$  (the temperature when VOC conversion is 50%) and  $T_{90}$  (the temperature when 90% of VOC has been converted).  $T_{50}$  is usually chosen as the main indicator of catalytic activity of a given catalyst. At  $T_{50}$  the catalytic activity is sufficiently high and the interactions between catalyst surface and reactants are intense. The lower  $T_{50}$  is, the higher is the catalytic activity of a catalyst. The three performance indices for acetone combustion are listed in Table 3. For  $T_{50}$ ,  $\text{SrMnO}_3$  and  $\text{La}_{0.6}\text{Pb}_{0.2}\text{Ca}_{0.2}\text{MnO}_3$  perovskites appear to be the most active catalysts on which the combustion of acetone became appreciable at 180–185 °C (50% conversion), and can quickly reach 95% conversion at 300 °C (Fig. 5). This catalytic performance is comparable to that of the  $\text{Pt}/\text{Al}_2\text{O}_3$  catalyst which could achieve the same conversion (95%) of acetone at 300 °C [47].

The time stability test of the catalytic activity was carried out for  $\text{La}_{0.6}\text{Pb}_{0.2}\text{Ca}_{0.2}\text{MnO}_3$  catalyst at reaction temperature of 250 °C for 36 h and for  $\text{SrMnO}_3$  catalyst at 200 °C for 30 h. By a continuous operation of the reactor, while periodically monitoring the conversion, very small variations of the conversion were obtained. As shown in Fig. 7, the catalytic performance of the two catalysts was maintained approximately constant (of about 90% and 64% respectively) throughout the test period. This result attests that the  $\text{La}_{0.6}\text{Pb}_{0.2}\text{Ca}_{0.2}\text{MnO}_3$  and  $\text{SrMnO}_3$  perovskites are active and stable catalysts.

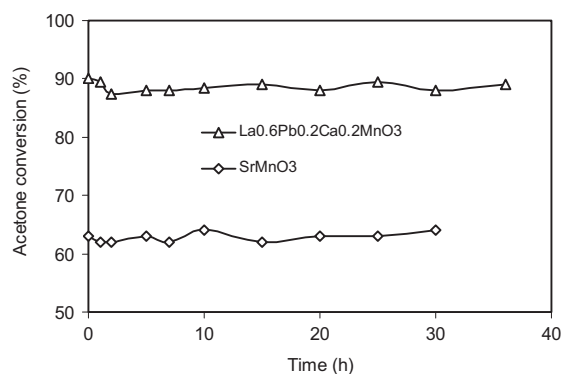


Fig. 7. Evolution of acetone conversion with time for the La<sub>0.6</sub>Pb<sub>0.2</sub>Ca<sub>0.2</sub>MnO<sub>3</sub> catalyst at 250 °C and for SrMnO<sub>3</sub> catalyst at 200 °C (acetone concentration 1–2% and GHSV=5100 h<sup>-1</sup>).

Table 3 also includes the values of the kinetic parameters (apparent activation energy,  $E_{app}$ , and reaction rate) for acetone oxidation over the six catalysts and the acetone conversion at 400 °C. The apparent activation energies ( $E_{app}$ ) for the catalytic combustion reaction of acetone were estimated from linear Arrhenius plots for low conversion regions. Note the wide variation in activation energies from 37 kJ/mol (SrMnO<sub>3</sub>) to 102 kJ/mol (CuFe<sub>2</sub>O<sub>4</sub>) toward acetone combustion. The smallest values of  $E_{app}$  for SrMnO<sub>3</sub> and La<sub>0.6</sub>Pb<sub>0.2</sub>Ca<sub>0.2</sub>MnO<sub>3</sub> perovskites offer an explanation for the best catalytic activity of these catalysts. The values of activation energies obtained by us are in good agreement with those reported for acetone combustion over Cu-doped ceria catalysts [48]. The  $E_{app}$  values fall within the common range of 37–102 kJ/mol and this suggests that the mechanism of the catalyzed reaction of acetone did not change over perovskite or ferrite catalysts having different crystalline structures and compositions, but rather changed the concentration of catalytically active sites involved in catalysis of acetone oxidation over the oxide compounds studied.

The reaction rate normalized to specific area can characterize the specific catalytic activity of catalysts. The higher the reaction rate is, the more active the catalyst is. From Table 3 one can remark that the reaction rate per square meter of catalyst substantially changes from  $1.35 \times 10^{-2}$  μmol/s m<sup>2</sup> (over Ni–Co ferrite) to  $140 \times 10^{-2}$  μmol/s m<sup>2</sup> (over SrMnO<sub>3</sub>). The highest values of the reaction rate were obtained for acetone combustion over perovskite catalysts which proved the best catalytic properties (95–97% conversion degree at 400 °C).

From Table 3 one can see that the catalytic activity at 400 °C of perovskite catalysts is better (91–97% conversion) than that of the spinel ferrites (81–89% conversion). The activities of the six catalysts (for acetone oxidation at 400 °C) decrease in the following series: La<sub>0.6</sub>Pb<sub>0.2</sub>Ca<sub>0.2</sub>MnO<sub>3</sub> > SrMnO<sub>3</sub> > FeMnO<sub>3</sub> > CuFe<sub>2</sub>O<sub>4</sub> > Ni<sub>0.5</sub>Co<sub>0.5</sub>Fe<sub>2</sub>O<sub>4</sub> > MgFe<sub>2</sub>O<sub>4</sub>. There is no obvious dependence of catalyst activity on surface specific area ( $S_{BET}$ ) given in Table 1.

The better catalyst performance of the perovskites compared to the ferrite catalysts under the same reaction conditions may be explained by the large increase in the oxygen vacancies in the surface regions generated by the presence of manganese ion with variable valence (Mn<sup>3+</sup>–Mn<sup>4+</sup>) [49]. Although the

mechanism of complete gas oxidation over metal oxide compounds is not precisely known, the interaction of surface active oxygen species with reactants (“suprafacial mechanism”) is a widely accepted explanation for the VOCs full oxidation over oxide catalysts for  $T \leq 400$  °C [50,51]. According to this opinion, the oxygen vacancies play an important role in the catalytic activity of the oxide catalysts, these being responsible for the adsorption/desorption properties of the gas phase. More oxygen vacancies will involve a larger density of adsorbed oxygen species (O<sup>-</sup>, O<sup>2-</sup>, O<sub>2</sub><sup>-</sup>), weakly anchored on the catalyst surface, which favor the VOCs oxidation. The larger the number of oxygen adsorbed, the more active would be the catalyst for gas oxidation.

#### 4. Conclusions

Two types of nanocrystalline oxide compounds, ferrosinels (CuFe<sub>2</sub>O<sub>4</sub>, MgFe<sub>2</sub>O<sub>4</sub>, Ni<sub>0.5</sub>Co<sub>0.5</sub>Fe<sub>2</sub>O<sub>4</sub>) and perovskites (SrMnO<sub>3</sub>, FeMnO<sub>3</sub>, La<sub>0.6</sub>Pb<sub>0.2</sub>Ca<sub>0.2</sub>MnO<sub>3</sub>), were prepared by sol–gel self-combustion method. The X-ray diffraction confirmed that all samples were monophasic and presented nanosized crystallinity (26–89 nm). The samples were catalytically tested in the flameless combustion reaction of diluted acetone in air. We analyzed comparatively the catalytic performances of these perovskites and ferrites. The results revealed a higher catalytic activity of the perovskite catalysts at low temperatures relative to that of ferrite catalysts. The acetone conversion degree over SrMnO<sub>3</sub> and La<sub>0.6</sub>Pb<sub>0.2</sub>Ca<sub>0.2</sub>MnO<sub>3</sub> perovskite catalysts can exceed 95% at 300 °C, whereas over ferrite catalysts this is much lower, of about 70%. A possible explanation for the higher activities of perovskites compared to those of spinels may be related to the specific features of their structures.

#### Acknowledgment

This work was supported by a grant of the Romanian National Authority for Scientific Research, CNST–UEFISCDI, project number PN-II-ID-PCE-2011-3-0453.

#### References

- [1] N. Fiedler, R. Robert Laumbach, K. Kelly-McNeil, P. Liroy, Z.-H. Fan, J. Zhang, J. Ottenweller, P. Ohman-Strickland, H. Kipen, Health effects of a mixture of indoor air volatile organics. Their ozone oxidation products and stress, *Environ. Health Perspect.* 113 (2005) 1542–1548.
- [2] Z. Fan, P. Liroy, C. Weschler, N. Fiedler, H. Kipem, J. Zhang, Ozone-initiated reactions with mixtures of volatile organic compounds under simulated indoor conditions, *Environ. Sci. Technol.* 37 (2003) 1811–1821.
- [3] L. Elsgaard, Ethylene removal at low temperatures under biofilter and batch conditions, *Appl. Environ. Microbiol.* 66 (2000) 3878–3882.
- [4] W.B. Li, J.X. Wang, H. Gong, Catalytic combustion of VOCs on non-noble metal catalysts, *Catal. Today* 148 (2009) 81–87.
- [5] R. Spinicci, A. Tofanari, A. Delmastro, D. Mazza, S. Ronchetti, Catalytic properties of stoichiometric and non-stoichiometric LaFeO<sub>3</sub> perovskite for total oxidation of methane, *Mater. Chem. Phys.* 76 (2002) 20–25.
- [6] J.J. Spivey, Complete catalytic oxidation of volatile organics, *Ind. Eng. Chem. Res.* 26 (1987) 2165–2180.

- [7] Y. Ma, M. Chen, C. Song, X. Zheng, Catalytic oxidation of toluene, acetone and ethyl acetate on a new Pt–Pd/stainless steel wire mesh catalyst, *Acta Phys. Chim. Sin.* 24 (2008) 1132–1136.
- [8] K. Everaert, J. Baeyens, Catalytic combustion of volatile organic compounds, *J. Hazard. Mater. B* 109 (2004) 113–139.
- [9] W.B. Li, W.B. Chu, M. Zhuang, J. Hua, catalytic oxidation of toluene on Mn-containing mixed oxides prepared in reverse microemulsions, *Catal. Today* 93–95 (2004) 205–209.
- [10] H.G. Ahn, B.M. Choi, D.J. Lee, Complete oxidation of ethylene over supported gold nanoparticle catalysts, *J. Nanosci. Nanotechnol.* 6 (2006) 3599–3603.
- [11] L. van de Beld, M.C. van der Ven, K.R. Westerterp, A kinetic study of the complete oxidation of ethane, propane and their mixtures on a Pd/Al<sub>2</sub>O<sub>3</sub> catalyst, *Chem. Eng. Process.* 34 (1995) 469–478.
- [12] A.K. Sinha, K. Suzuki, M. Takahara, H. Azuma, T. Nonaka, K. Fukumoto, Mesoporous manganese oxide/gold nanoparticle composites for extensive air purification, *Angew. Chem. Int. Ed.* 46 (2007) 2891–2894.
- [13] S.C. Kim, W.G. Shim, Catalytic combustion of VOCs over a series of manganese oxide catalysts, *Appl. Catal. B* 98 (2010) 180–185.
- [14] A.K. Sinha, K. Suzuki, Three-dimensional mesoporous chromium oxide: a highly efficient material for the elimination of volatile organic compounds, *Angew. Chem. Int. Ed.* 44 (2005) 271–273.
- [15] J. Luo, Q. Zhang, A. Huang, S.L. Suib, Total oxidation of volatile organic compounds with hydrophobic cryptomelane-type octahedral molecular sieves, *Microporous Mesoporous Mater.* 35–36 (2000) 209–217.
- [16] H. Chen, X. Tony, Y. Li, Mesoporous Cu–Mn Hopcalite catalyst and its performance in low temperature ethylene combustion in a carbon dioxide stream, *Appl. Catal., A* 370 (2009) 59–65.
- [17] D. Kim, S. Ihm, Application of spinel-type cobalt chromite as a novel catalyst for combustion of chlorinated organic pollutants, *Environ. Sci. Technol.* 35 (2001) 222–226.
- [18] Z. Mu, J.J. Li, M.H. Duan, Z.P. Hao, S.Z. Qiao, Catalytic combustion of benzene on Co/CeO<sub>2</sub>/SBA-15 and Co/SBA-15 catalysts, *Catal. Commun.* 9 (2008) 1874–1877.
- [19] K. Jiráková, J. Mikulová, J. Klempa, T. Grygar, Z. Bastl, F. Kovanda, Modification of Co–Mn–Al mixed oxide with potassium and its effect on deep oxidation of VOC, *Appl. Catal., A* 361 (2009) 106–116.
- [20] T.K. Tseng, L. Wang, C.T. Ho, H. Chu, The destruction of dichloroethane over a gamma-alumina supported manganese oxide catalyst, *J. Hazard. Mater.* 178 (2010) 1035–1040.
- [21] M.R. Morales, B.P. Barbero, L.E. Cadús, Evaluation and characterization of Mn–Cu mixed oxide catalysts for ethanol total oxidation: influence of copper content, *Fuel* 87 (2008) 1177–1186.
- [22] M. Baldi, E. Finocchio, F. Milella, G. Busca, Catalytic combustion of C<sub>3</sub> hydrocarbons and oxygenates over Mn<sub>3</sub>O<sub>4</sub>, *Appl. Catal. B* 16 (1998) 43–51.
- [23] L.G. Tejuca, J.L.G. Fierro, J.M.O. Tascon, Structure and reactivity of perovskite-type oxides, *Adv. Catal.* 36 (1989) 327–328.
- [24] N. Yamazoe, Y. Teraoka, Oxidation catalysis of perovskites–relationships to bulk structure and composition (valency, defect, etc.), *Catal. Today* 8 (1990) 175–199.
- [25] T. Seiyama, Total oxidation of hydrocarbons on perovskite, *Catal. Rev. Sci. Eng.* 34 (1992) 281–300.
- [26] A. Musialiak-Piotrowska, K. Syczewska, Combustion of volatile organic compounds in two-component mixtures over monolithic perovskite catalysts, *Catal. Today* 59 (2000) 269–278.
- [27] M.A. Pena, J.L.G. Fierro, Chemical structure and performance of perovskite oxides, *Chem. Rev.* 101 (2001) 1981–2018.
- [28] A. Urda, A. Herraiz, A. Rédey, I.C. Marcu, Co and Ni ferrosinels as catalysts for propane total oxidation, *Catal. Commun.* 10 (2009) 1651–1655.
- [29] M. Florea, M. Alifanti, V.I. Parvulescu, D. Mihaila-Tarabasanu, L. Diamandescu, M. Feder, C. Negrilă, L. Frunza, Total oxidation of toluene on ferrite-type catalysts, *Catal. Today* 14 (2009) 361–366.
- [30] A.S. Albuquerque, M.V.C. Tolentino, J.C. Aldrisson, F.C.C. Moura, Renato de Mendonça, W.A.A. Macedom, Nanostructured ferrites: structural analysis and catalytic activity, *Ceram. Int.* 38 (2012) 2225–2231.
- [31] C.C. Ramakutty, S. Sugunan, Surface properties and catalytic activity of ferrosinels of nickel, cobalt and copper, prepared by soft chemical methods, *Appl. Catal. A* 218 (2001) 39–51.
- [32] P. Jacobs, A. Maltha, J. Drimal, V. Ponec, H.H. Brongersma, The surface of catalytically active spinels, *J. Catal.* 47 (1994) 294–300.
- [33] N. Chu, X. Wang, J.G.H. Reijts, Y. Liu, H. Jin, Q. Wu, L. Li, Z. Wang, H. Ge, Magnetic properties of low Mn-doped NiCuZn nanocrystalline ferrites, *J. Alloys Compd.* 470 (2009) 438–442.
- [34] A.B. Gadkari, T.J. Shinde, P.N. Vasambekar, Structural analysis of Y<sup>3+</sup> doped Mg–Cd ferrites prepared by oxalate co-precipitation method, *Mater. Chem. Phys.* 114 (2009) 505–510.
- [35] X. Li, G. Wang, Low-temperature synthesis and growth of superparamagnetic Zn<sub>0.5</sub>Ni<sub>0.5</sub>Fe<sub>2</sub>O<sub>4</sub> nanosized particles, *J. Magn. Magn. Mater.* 321 (2009) 1276–1279.
- [36] A.C.F.M. Costa, R.T. Lula, R.H.G.A. Kiminami, L.F.V. Gama, A.A. de Jesus, H.M.C. Andrade, Preparation of nanostructured NiFe<sub>2</sub>O<sub>4</sub> catalysts by combustion reaction, *J. Mater. Sci.* 41 (2006) 4871.
- [37] C. Oliva, L. Bonoldi, S. Cappelli, L. Fabbrini, I. Rossetti, L. Forni, Effect of preparation parameters on SrTiO<sub>3</sub> +/– delta catalyst for the flameless combustion of methane, *J. Mol. Catal. A: Chem.* 226 (2005) 33–40.
- [38] P.D. Popa, N. Rezlescu, Gh. Iacob, A New Procedure for Preparing Ferrite Powders, Romanian Patent No. 121300, OSIM, Bucharest, 2008.
- [39] N. Rezlescu, E. Rezlescu, L. Sachelarie, P.D. Popa, C. Doroftei, Structural and catalytic properties of mesoporous nanocrystalline mixed oxides containing magnesium, *Catal. Commun.* 46 (2014) 51–56.
- [40] N. Rezlescu, E. Rezlescu, L. Sachelarie, P.D. Popa, C. Doroftei, M. Ignat, Nanocrystalline mixed oxides containing magnesium prepared by a combined sol–gel and self-combustion method for catalyst applications, *Mater. Sci. Appl.* 4 (2013) 447–452.
- [41] S. Lowell, J.E. Shields, M.A. Thomas, M. Thommes, Characterization of Porous Solids and Powders: Surface Area, Pore Size and Density, Kluwer Academic Publishers, Dordrecht/Boston/London, 2004.
- [42] N. Rezlescu, E. Rezlescu, P.D. Popa, C. Doroftei, M. Ignat, Nanostructured GdAlO<sub>3</sub> perovskite, a new possible catalyst for combustion of volatile organic compounds, *J. Mater. Sci.* 48 (2013) 4297–4304.
- [43] R. Mahendiran, R. Mahesh, A.K. Raychaudhuri, C.N.R. Rao, Room-temperature giant magnetoresistance in La<sub>1–x</sub>Pb<sub>x</sub>MnO<sub>3</sub>, *Phys. D: Appl. Phys.* 28 (1995) 1743–1745.
- [44] N.G. Pirogova, N.M. Panich, R.I. Korosteleva, Yu.V. Voronin, G. E. Kalinina, Catalytic properties of ferrites in oxidation reactions, *Russ. Chem. Bull.* 45 (1996) 42–44.
- [45] A. Kaddouri, P. Gelin, N. Dupont, Methane catalytic combustion over La–Ce–Mn–O-perovskite prepared using dielectric heating, *Catal. Commun.* 10 (2009) 1085–1089.
- [46] R.M.G. de la Cruz, H. Falcon, M.A. Pena, J.L.G. Fierro, Role of bulk and surface structures of La<sub>1–x</sub>Sr<sub>x</sub>NiO<sub>3</sub> perovskite-type oxides in methane combustion, *Appl. Catal. B: Environ.* 33 (2001) 45–55.
- [47] N. Burgos, M. Paulis, M.M. Antxustegi, M. Montes, Deep oxidation of VOC mixtures with platinum supported on Al<sub>2</sub>O<sub>3</sub>/Al monoliths, *Appl. Catal. B-Environ.* 38 (2002) 251–258.
- [48] Ch. Hu, Q. Zhu, Z. Jiang, L. Chen, R. Wu, Catalytic combustion of dilute acetone over Cu-doped ceria catalysts, *Chem. Eng. J.* 152 (2009) 583–590.
- [49] N. Rezlescu, E. Rezlescu, P.D. Popa, C. Doroftei, M. Ignat, Characterization and catalytic properties of some perovskites, *Composites Part B: Eng.* 60 (2014) 515–522.
- [50] D.V. Ivanov, L.G. Pinaeva, E.M. Sadovskaya, L.A. Isupova, Influence of the mobility of oxygen on the reactivity of La<sub>1–x</sub>Sr<sub>x</sub>MnO<sub>3</sub> perovskites in methane oxidation, *Kinet. Catal.* 52 (2011) 401–408.
- [51] D. Hirabayashi, T. Yosikawa, Y. Kawamoto, K. Mockizuki, K. Suzuki, Characterization and applications of calcium ferrites based materials containing active oxygen species, *Adv. Sci. Technol.* 45 (2006) 2169–2175.